communications physics

A Nature Portfolio journal

Article

https://doi.org/10.1038/s42005-025-02258-z

Spatial-mode diversity and multiplexing for continuous variables quantum communications

Seid Koudia [1] ✉, Leonardo Oleynik[1], Junaid ur Rehman [2] & Symeon Chatzinotas [1]

Quantum communication is a key enabler of future secure networks, but its performance is often limited by noise, channel fading, and interference. Current systems struggle to maintain high fidelity and key rates under realistic, dynamic channel conditions. Here, we show that continuous-variable quantum communication systems can benefit significantly from spatial-mode diversity combined with tailored amplification strategies, depending on the available knowledge of the channel. We model the effects of fading as a log-normal distribution and evaluate different amplification approaches at the transmitter and receiver. Our results demonstrate improved fidelity and robustness against noise and fading, especially in harsh environments. We also find that, in certain conditions, spatial-mode diversity provides higher secret key rates than conventional multiplexing strategies in continuous-variable quantum key distribution. These findings highlight the potential of diversity techniques to enhance the stability and scalability of quantum communication networks in practical deployments.

Continuous Variable (CV) quantum communications have emerged as a powerful and versatile approach to secure information transfer[1], encompassing both Quantum Key Distribution (QKD) and entanglement-based communications[2]. Unlike discrete variable systems, which rely on single photons, CV quantum communications utilize the continuous properties of light, such as amplitude and phase quadratures, offering distinct advantages in terms of implementation and integration with existing telecommunications infrastructure[3,4].

In the realm of Quantum Key Distribution, CV-QKD protocols provide a robust framework for generating and distributing cryptographic keys with unconditional security[5], rooted in the principles of quantum mechanics. These protocols leverage Gaussian-modulated coherent states and homodyne or heterodyne detection techniques[6], making them compatible with standard optical components and allowing for potentially higher key rates compared to their discrete variable counterparts[7] in practical cases concerning quantum-classical coexistence. Furthermore, CV-QKD systems can operate at room temperature and do not require the use of single-photon detectors, which simplifies their deployment and reduces costs[8–10].

Entanglement-based communications[11], on the other hand, exploit the fundamental properties of quantum entanglement to enable applications such as quantum teleportation, dense coding, and distributed quantum computing. CV entanglement offers the advantage of generating and manipulating entangled states with relatively high efficiency and fidelity, facilitating the creation of long-distance quantum networks[12].

One of the key challenges in CV quantum communications is the inherent sensitivity to noise and losses, which can significantly degrade the performance of quantum protocols. To address these issues and enhance the reliability and efficiency of CV quantum communication systems, two pivotal strategies can be identified: multiplexing and diversity.

Multiplexing techniques[4], including wavelength-division multiplexing (WDM)[13], mode-division multiplexing (MDM)[14] and Spatial multiplexing (SM)[15], enable the simultaneous transmission of multiple quantum channels over multicore/multimode fibers and free space links affected by crosstalk[16]. This approach not only increases the overall communication rates but also optimizes the utilization of available bandwidth, thereby enhancing the scalability of quantum networks. By integrating multiplexing methods, it is possible to achieve higher data throughput and more efficient use of resources, which is crucial for the practical deployment of large-scale quantum communication systems[4].

Diversity, on the other hand, plays a critical role in mitigating the effects of noise and losses, which are inevitable in real-world communication channels. Techniques such as spatial diversity, where signals are transmitted over multiple spatially separated paths, and temporal diversity, where information is spread over time slots, are widely used in classical communications to combat fading and ensure robustness. These principles have begun to be explored in quantum communications as well[17–19], particularly in continuous-variable (CV) settings where

[1]Interdisciplinary Center for Security Reliability and Trust (SnT), The university of Luxembourg, Luxembourg, Luxemburg. [2]Department of Electrical Engineering, King Fahd University of Petroleum and Minerals (KFUPM), Dhahran, Saudi Arabia. ✉e-mail: seid.koudia@uni.lu

Gaussian states and homodyne/heterodyne detection allow for practical implementations.

In the quantum domain, diversity can be implemented by transmitting quantum information through multiple independent spatial paths or modes, or by leveraging orthogonal degrees of freedom such as polarization, time-bin, or frequency. The goal is to reduce the likelihood that all paths suffer from simultaneous degradation – thereby enhancing the reliability and resilience of the quantum channel. Importantly, these strategies help mitigate not only random environmental fluctuations, such as atmospheric turbulence or thermal noise, but also targeted disruptions, which are relevant in adversarial settings like QKD.

However, a key limitation arises from the no-cloning theorem, which prohibits copying unknown quantum states. This makes straightforward redundancy schemes (e.g., duplication across paths) infeasible. To address this, recent work has proposed using asymmetric quantum cloning to distribute quantum information across paths in a way that retains partial fidelity while enabling diversity-like behavior[18].

Among various diversity strategies in quantum communication, spatial-mode diversity–explored in this work–entails transmitting quantum states over multiple spatially separated optical modes or physical paths, such as distinct cores, beams, or channels, within the same link. This approach reduces the impact of deep fading or noise on a single mode by enabling either statistical averaging or coherent recombination at the receiver. In contrast, site diversity, as studied in ref. 19, involves deploying multiple geographically distributed optical ground stations (OGSs) to mitigate channel interruptions caused by cloud cover or local atmospheric conditions. The key difference lies in the physical scale: spatial-mode diversity operates at the link level, improving the quality and stability of a single quantum channel, whereas site diversity improves overall link availability in satellite-based QKD systems by increasing the probability that at least one station is available during satellite overpasses.

Both methods share the core principle of exploiting statistical independence across parallel channels–be they spatial modes or geographic sites–to enhance system robustness. In free-space or satellite QKD scenarios, where high loss and weather-induced intermittency are major limitations, spatial-mode diversity can complement site diversity by stabilizing the quantum signal when a ground station is available. Thus, while the mechanisms differ in scope and implementation, the two forms of diversity are not only compatible but potentially synergistic in a global-scale quantum communication architecture.

In this paper, diversity schemes, involving multiple transmission paths and varying channel parameters, have been proposed to enhance the robustness of quantum communication systems. We examine the effectiveness of such schemes in CV quantum communications by considering the impact of fading, modeled as a log-normal distribution, and crosstalk. We quantify the performance improvements in terms of fidelity and secret key rate, an essential metric for the evaluation of CV-QKD systems.

Results

We analyze a single diversity-based communication scheme under three distinct amplification strategies, each corresponding to different assumptions about channel state information (CSI) available at the transmitter or receiver. In the context of this work, CSI refers to knowledge of the average statistical behavior of the channel–specifically, the average transmittivity $\langle T \rangle$ of the Gaussian lossy channel. This information can be obtained through classical channel estimation techniques, such as pilot-assisted measurements or pre-characterization of the channel in a quasi-static setting. Such statistical CSI does not imply instantaneous knowledge of channel fluctuations but rather an understanding of the long-term fading distribution parameters (e.g., log-normal mean and variance).

When the receiver possesses such CSI, it can apply one of two amplification strategies: (1) post-amplification, where active (phase-insensitive) amplification is applied to the quantum state before measurement to compensate for expected loss, or (2) postprocessing amplification, where amplification is applied classically to the measurement outcomes to mitigate signal degradation without interacting with the quantum state directly. In this scheme, postprocessing amplification refers to a purely classical operation performed on the measurement outcomes at the receiver. It consists of rescaling the detected quadrature values by a gain factor G, based on the estimated channel statistics. Since this operation occurs after measurement, it does not interact with the quantum state and therefore does not affect the covariance matrix. Only the first moment (mean displacement vector) is modified. In contrast, when CSI is available at the transmitter, a pre-amplification scheme can be employed. Here, the transmitter boosts the signal prior to sending it through the channel, effectively pre-compensating for expected losses.

These three schemes are illustrated in Fig. 1. The beam splitter parameter η plays a key role in the system architecture:

- At the transmitter side, the beam splitter with parameter η is used to split the input signal into two parts, which are then sent through two independent and identically distributed (i.i.d.) fading channels, thus enabling spatial-mode diversity.
- At the receiver side, a beam splitter (also parameterized by η) recombines the two received signals to form a single output mode that is subsequently measured, while the other output is discarded and treated as loss. This recombination process is designed to exploit constructive interference and statistical averaging between the two independently faded channels, thereby reducing the impact of channel fluctuations. The recombination process aims to exploit constructive interference and averaging effects to reduce the impact of channel fluctuations. Moreover, processing a single recombined mode aligns with typical assumptions in CV quantum communication protocols and simplifies both implementation and analytical treatment, while still capturing the benefits of spatial-mode diversity.
- This architecture assumes that the fading across the two paths is statistically independent and leverages spatial diversity to enhance robustness. Such a setup is especially relevant in quantum communication contexts–such as CV-QKD and entanglement-based protocols–where reliable transmission and minimal information loss are critical.

Postprocessing amplification

We assume that the Receiver has a CSI regarding the average behavior of the fading channel. As such, he might apply post-processing amplification after performing a heterodyne measurement on the quadratures of the received signal. This is valid when transmitting classical information encoded in the

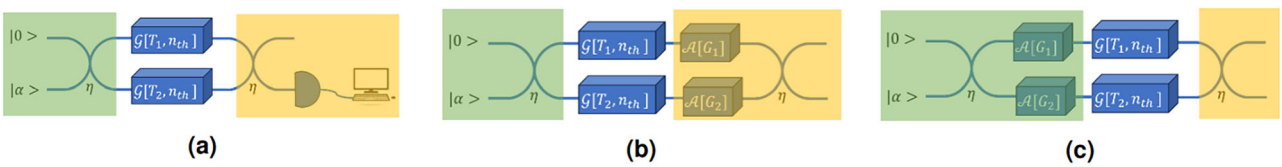

Fig. 1 | A diversity scheme with different amplification techniques. The green and yellow shadowed boxes refer to the operations carried by the transmitter and the receiver, respectively. **a** A diversity scheme with postprocessing amplification of the signal upon CSI at the receiver. **b** A diversity scheme with postamplification of the signal upon CSI at the receiver. **c** A diversity scheme with preamplification of the signal with CSI at the transmitter.

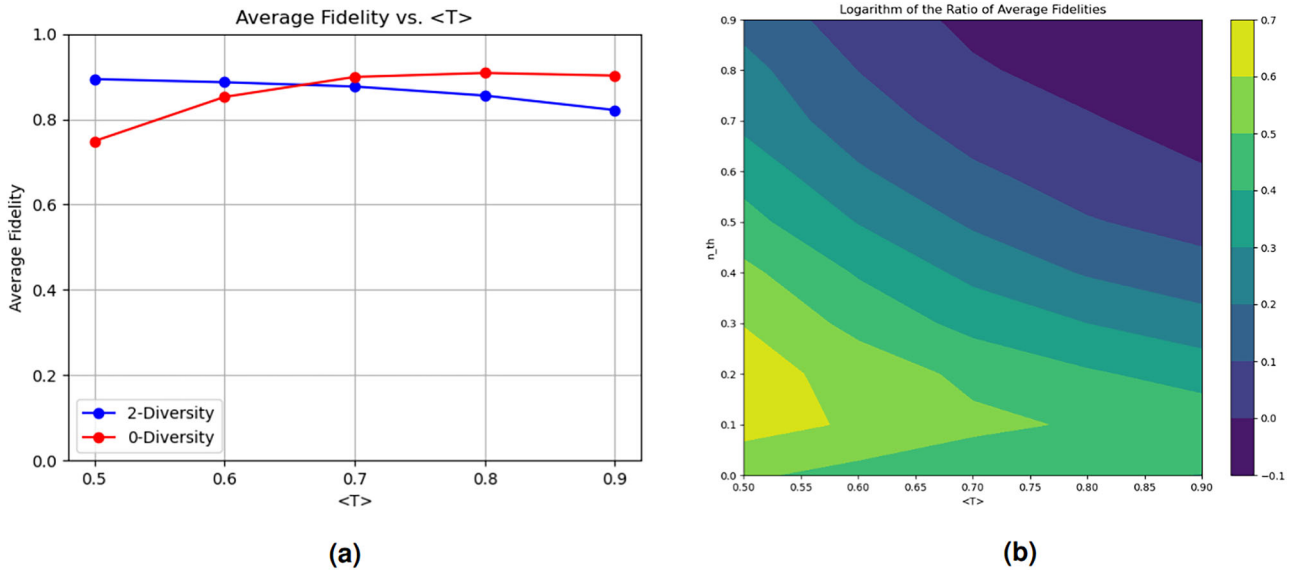

Fig. 2 | The behavior of the average fidelity when the diversity scheme is employed with postprocessing amplification. a The average fidelity in the 2-diversity and the 0-diversity schemes as a function of the average transmissivity $<T>$ of the fading channel for $n_{th} = 0.9$ for the thermal Gaussian noise. **b** The log scale of the ratio between the average fidelities in the 2-diversity and the 0-diversity schemes as a function of the average transmissivity of the fading channels and the strength of the thermal Gaussian noise.

quadratures of the Gaussian state. This postprocessing amplification does not interact with the signal actively; hence, it does not introduce any additional noise or corrections to the covariance matrix, although it does only rescale the output state's quadratures

$$\vec{d} \rightarrow G\vec{d} \tag{1}$$

where G is the postprocessing amplification gain. The global evolution of the system is given by:

$$\begin{aligned} V_1 \oplus V_2 \rightarrow & B(\eta)\left[(K_1 \oplus K_2)(V_1 \oplus V_2)(K_1 \oplus K_2)^T\right. \\ & \left.+(N_1 \oplus N_2)\right]B(\eta)^T \\ d_1 \oplus d_2 \rightarrow & G \cdot B(\eta)(K_1 \oplus K_2)(d_1 \oplus d_2) \end{aligned} \tag{2}$$

where $\oplus$ stands for the direct sum. The covariance matrix of the states evolves after the described process as follows:

$$V_{in}^{(2)} = \begin{pmatrix} \frac{\mathrm{I}_2}{2} & 0 \\ 0 & \frac{\mathrm{I}_2}{2} \end{pmatrix} \rightarrow V_{out}^{(2)} = \begin{pmatrix} V1 & V2 \\ V2 & V3 \end{pmatrix} \tag{3}$$

where

$$V1 = (\eta B_1 + (1-\eta)B_2)\mathrm{I}_2 \tag{4}$$

$$V2 = (\sqrt{\eta(1-\eta)}(B_1 - B_2))\mathrm{I}_2 \tag{5}$$

$$V_3 = (\eta B_2 + (1-\eta)B_1)\mathrm{I}_2 \tag{6}$$

with

$$B_1 = T_1\left(\frac{1}{2} - \left(n_{th} + \frac{1}{2}\right)\right) + \left(n_{th} + \frac{1}{2}\right) \tag{7}$$

$$B_2 = T_2\left(\frac{1}{2} - \left(n_{th} + \frac{1}{2}\right)\right) + \left(n_{th} + \frac{1}{2}\right) \tag{8}$$

The mean vectors evolve according to the described process as:

$$\begin{aligned} d_1 = 0 \rightarrow & \left[\left(\sqrt{\eta T_1}\frac{x}{\sqrt{2\langle T_1\rangle}} - \sqrt{(1-\eta)T_2}\frac{x}{\sqrt{2\langle T_1\rangle}}\right)\right. \\ & \left.+i\left(\sqrt{\eta T_1}\frac{p}{\sqrt{2\langle T_1\rangle}} - \sqrt{(1-\eta)T_2}\frac{p}{\sqrt{2\langle T_1\rangle}}\right)\right] \\ d_2 = x + ip \rightarrow & \left[\left(\sqrt{\eta T_2}\frac{x}{\sqrt{2\langle T_2\rangle}} + \sqrt{(1-\eta)T_1}\frac{x}{\sqrt{2\langle T_2\rangle}}\right)\right. \\ & \left.+i\left(\sqrt{\eta T_2}\frac{p}{\sqrt{2\langle T_2\rangle}} + \sqrt{(1-\eta)T_1}\frac{p}{\sqrt{2\langle T_2\rangle}}\right)\right] \end{aligned} \tag{9}$$

The results for fixed thermal background noise to $n_{th} = 0.9$ are shown in Fig. 2a. We notice that a 2-diversity scheme is performing better than single transmission in very strong fading channels. We stress that the advantage also depends on the thermal background noise. This dependence is highlighted in Fig. 2b.

Post-amplification

We assume that CSI about the average behavior of the fading is available to the receiver. Accordingly, he makes a post-amplification to overcome the effect of losses. This postamplification mechanism is different from the postprocessing mechanism, as this one allows the receiver to actively interact with the signal. Therefore, an additional noise to the covariance of the signal is unavoidable. Indeed, the strength of the fading can be different in the two channels, hence different amplification gains should be applied depending on the individual CSI. The global evolution of the system is given by:

$$\begin{aligned} & V_1 \oplus V_2 \rightarrow \\ & B(\eta)\left[(A(G_1)\oplus A(G_2))\left[(K_1 \oplus K_2)(V_1 \oplus V_2)(K_1 \oplus K_2)^T\right.\right. \\ & \left.\left.+(N_1 \oplus N_2)\right](A(G_1)\oplus A(G_2))^T + N_{A(G_1)} \oplus N_{A(G_2)}\right]B(\eta)^T \\ & d_1 \oplus d_2 \rightarrow B(\eta)(A(G_1)\oplus A(G_2))(K_1 \oplus K_2)(d_1 \oplus d_2) \end{aligned} \tag{10}$$

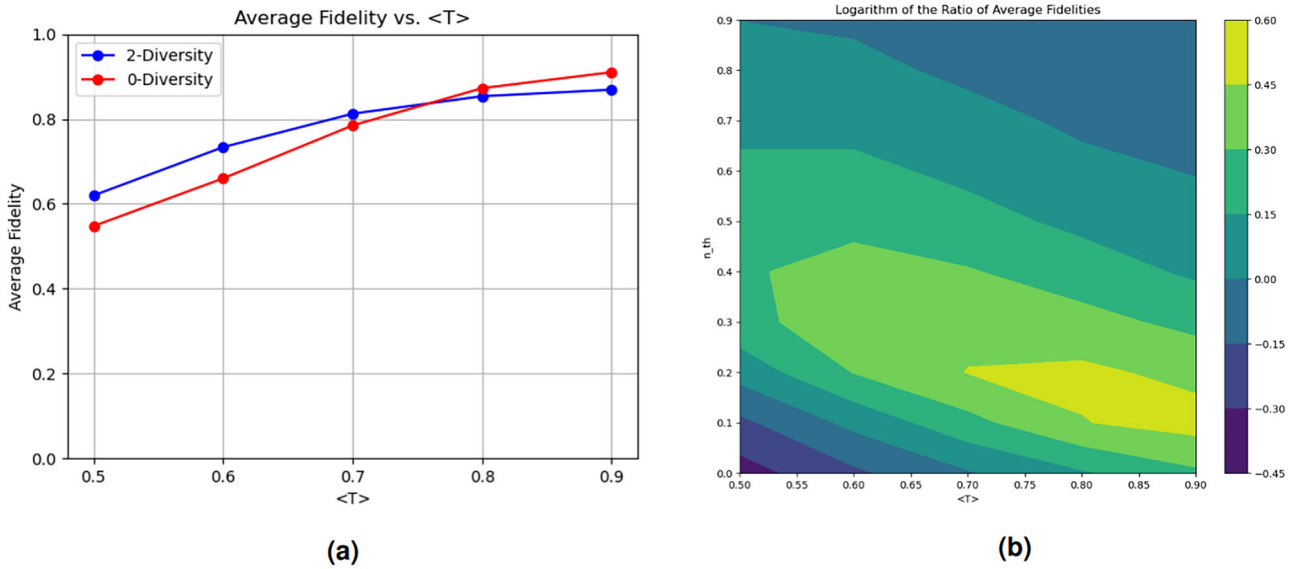

Fig. 3 | The behavior of the average fidelity when the diversity scheme is employed with post-amplification. a The average fidelity in the 2-diversity and the 0-diversity schemes as a function of the average transmissivity $<T>$ of the fading channel for $n_{th} = 0.7$ for the thermal Gaussian noise. **b** The log scale of the ratio between the average fidelities in the 2-diversity and the 0-diversity schemes as a function of the average transmissivity of the fading channels and the strength of the thermal Gaussian noise.

Explicitly, the covariance matrix evolves as:

$$V_{in}^{(2)} = \begin{pmatrix} \frac{I_2}{2} & 0 \\ 0 & \frac{I_2}{2} \end{pmatrix} \rightarrow V_{out}^{(2)} = \begin{pmatrix} V1 & V2 \\ V2 & V3 \end{pmatrix}$$

$$V1 = (\eta B_1 + (1-\eta)B_2)\mathrm{I}_2 \tag{11}$$

$$V2 = (\sqrt{\eta(1-\eta)}(B_1 - B_2))\mathrm{I}_2 \tag{12}$$

$$V_3 = (\eta B_2 + (1-\eta)B_1)\mathrm{I}_2 \tag{13}$$

with

$$B_1 = G_1\left[T_1\left(\frac{1}{2} - \left(n_{th} + \frac{1}{2}\right)\right) + \left(n_{th} + \frac{1}{2}\right)\right] + \frac{G_1 - 1}{2} \tag{14}$$

$$B_2 = G_2\left[T_2\left(\frac{1}{2} - \left(n_{th} + \frac{1}{2}\right)\right) + \left(n_{th} + \frac{1}{2}\right)\right] + \frac{G_2 - 1}{2} \tag{15}$$

where G_1 and G_2 are the amplification gains. The mean vectors evolve according to the described process as:

$$\begin{aligned} d_1 =& 0 \rightarrow \left[\left(\sqrt{\eta T_1}\frac{x}{\sqrt{2\langle T_1\rangle}} - \sqrt{(1-\eta)T_2}\frac{x}{\sqrt{2\langle T_1\rangle}}\right)\right. \\ &\left. + i\left(\sqrt{\eta T_1}\frac{p}{\sqrt{2\langle T_1\rangle}} - \sqrt{(1-\eta)T_2}\frac{p}{\sqrt{2\langle T_1\rangle}}\right)\right] \\ d_2 =& x + ip \rightarrow \left[\left(\sqrt{\eta T_2}\frac{x}{\sqrt{2\langle T_2\rangle}} + \sqrt{(1-\eta)T_1}\frac{x}{\sqrt{2\langle T_2\rangle}}\right)\right. \\ &\left. + i\left(\sqrt{\eta T_2}\frac{p}{\sqrt{2\langle T_2\rangle}} + \sqrt{(1-\eta)T_2}\frac{p}{\sqrt{2\langle T_2\rangle}}\right)\right] \end{aligned} \tag{16}$$

A benchmark between the average fidelity in 2-diversity and 0-diversity schemes is highlighted in Fig. 3a. Indeed, the diversity advantage depends on the average behavior of the fading channel and on the background thermal noise. The benchmarking of the two schemes regarding both degrees of freedom of the channel is illustrated in Fig. 3b.

Pre-amplification

We assume that CSI about the average behavior of the fading is available to the transmitter. Accordingly, he makes a pre-amplification to overcome the effect of losses at the expense of adding additional noise to the system. The evolution of the covariance matrix and the mean vectors in such a setup is given by:

$$\begin{aligned} &V_1 \oplus V_2 \rightarrow \\ &B(\eta)\left[(K_1 \oplus K_2)\left[(A(G_1) \oplus A(G_2))(V_1 \oplus V_2)(A(G_1) \oplus A(G_2))^T\right.\right. \\ &\left.\left. + N_{A(G_1)} \oplus N_{A(G_2)}\right](K_1 \oplus K_2)^T + (N_1 \oplus N_2)\right]B(\eta)^T \end{aligned} \tag{17}$$

$$d_1 \oplus d_2 \rightarrow B(\eta)(K_1 \oplus K_2)(A(G_1) \oplus A(G_2))(d_1 \oplus d_2) \tag{18}$$

Explicitly,

$$V_{in}^{(2)} = \begin{pmatrix} \frac{I_2}{2} & 0 \\ 0 & \frac{I_2}{2} \end{pmatrix} \rightarrow V_{out}^{(2)} = \begin{pmatrix} V1 & V2 \\ V2 & V3 \end{pmatrix} \tag{19}$$

$$V1 = (\eta B_1 + (1-\eta)B_2)\mathrm{I}_2 \tag{20}$$

$$V2 = \left(\sqrt{\eta(1-\eta)}(B_1 - B_2)\right)\mathrm{I}_2 \tag{21}$$

$$V_3 = (\eta B_2 + (1-\eta)B_1)\mathrm{I}_2 \tag{22}$$

with

$$B_1 = (2G_1 - 1)\frac{T_1}{2} + (1 - T_1)\left(n_{th} + \frac{1}{2}\right) \tag{23}$$

$$B_2 = (2G_2 - 1)\frac{T_2}{2} + (1 - T_2)\left(n_{th} + \frac{1}{2}\right) \tag{24}$$

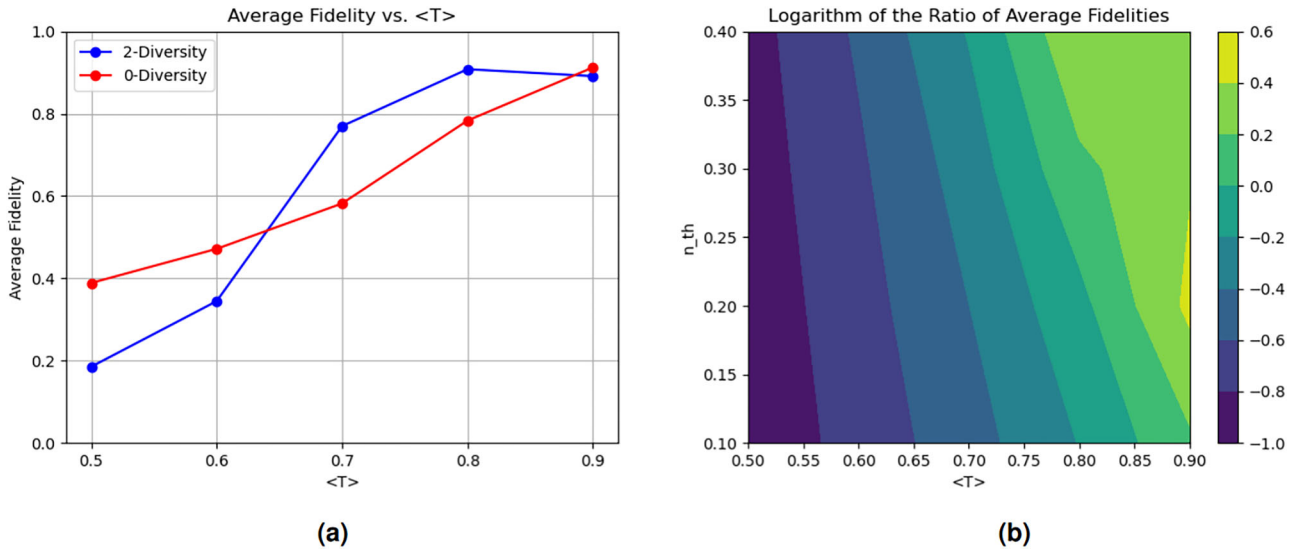

Fig. 4 | The behavior of the average fidelity when the diversity scheme is employed with pre-amplification. a The average fidelity in the 2-diversity and the 0-diversity schemes as a function of the average transmissivity $<T>$ of the fading channel for $n_{th} = 0.7$ for the thermal Gaussian noise. **b** The log scale of the ratio between the average fidelities in the 2-diversity and the 0-diversity schemes as a function of the average transmissivity of the fading channels and the strength of the thermal Gaussian noise.

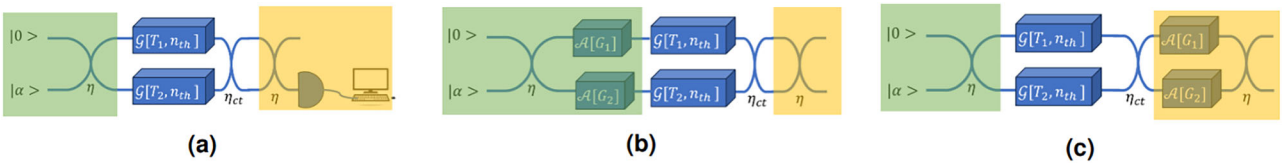

Fig. 5 | A diversity scheme with different amplification techniques in the presence of cross talk. The green and yellow shadowed boxes refer to the operations carried by transmitter and the receiver respectively. **a** A diversity scheme with postprocessing amplification of the signal upon CSI at the receiver. **b** A diversity scheme with postamplification of the signal upon CSI at the receiver. **c** A diversity scheme with preamplification of the signal with CSI at the transmitter.

where G_1 and G_2 are the amplification gains. The mean vectors evolve according to the described processs as:

$$\begin{aligned} d_1 =0 \to & \left[\left(\sqrt{\eta T_1}\frac{x}{\sqrt{2\langle T_1\rangle}} - \sqrt{(1-\eta)T_2}\frac{x}{\sqrt{2\langle T_1\rangle}}\right)\right. \\ & \left. +i\left(\sqrt{\eta T_1}\frac{p}{\sqrt{2\langle T_1\rangle}} - \sqrt{(1-\eta)T_2}\frac{p}{\sqrt{2\langle T_1\rangle}}\right)\right] \\ d_2 =x+ip \to & \left[\left(\sqrt{\eta T_2}\frac{x}{\sqrt{2\langle T_2\rangle}} + \sqrt{(1-\eta)T_1}\frac{x}{\sqrt{2\langle T_2\rangle}}\right)\right. \\ & \left. +i\left(\sqrt{\eta T_2}\frac{p}{\sqrt{2\langle T_2\rangle}} + \sqrt{(1-\eta)T_2}\frac{p}{\sqrt{2\langle T_2\rangle}}\right)\right] \end{aligned} \tag{25}$$

A comparison between the 2-diversity and 0-diversity schemes is illustrated in Fig. 4a for a fixed thermal noise and Fig. 4b for a varying thermal noise. A clear reduction in the advantage of diversity is witnessed with respect to the previous amplification methods, especially in the regime of strong fading and thermal noise.

In the presence of cross talk

We model crosstalk in CV quantum communications as a beam splitter with a stochastic transmissivity parameter as discussed in **Methods**. In the presence of crosstalk, the covariances and the mean vector of the system undergo the global evolution given in Eqs. (26)–(28). Therein, $B(\eta_{ct})$ denotes the crosstalk noise between the two channels, with η_{ct} being the crosstalk parameters reflecting the strength of the interference between the transmitted signals. The diversity scheme with different amplification methods employed in the presence of crosstalk is illustrated in Fig. 5. The simulations are presented in Fig. 6a, b, and, c, respectively for postprocessing amplification, postamplification, and preamplification. We note that in the presence of cross-talk, the advantage brought by the 2-diversity scheme is reduced for postprocessing, postamplification, and pre-amplification, respectively, but an advantage is still observed at strong fading and strong cross-talk for postprocessing and post-amplification. In the contrary, no advantage is witnessed for post-amplification in the presence of crosstalk. This reflects the fact that in postamplification, the noise in the transmission paths, be it loss or thermal, is amplified along with the signal, leading to a noisy state at the output.

Secret key rate

A direct consequence of the fidelity increase brought by the diversity scheme is the possibility to decrease the probability of error of decoding a given state, resulting in a higher secret key rate in CV-QKD. To study this, we consider the same prepare and measure scenario used until now, where Alice, the transmitter, prepares coherent states modulated using a centered bivariate Gaussian distribution in phase space, with variance V_{in}. This is consistent with the standard Gaussian modulation protocol used in CV-QKD.

$$\begin{aligned} V_1 \oplus V_2 &\to B(\eta)B(\eta_{ct})\left[(K_1 \oplus K_2)(V_1 \oplus V_2)(K_1 \oplus K_2)^T + (N_1 \oplus N_2)\right]B(\eta_{ct})^T B(\eta)^T \\ d_1 \oplus d_2 &\to G \cdot B(\eta)B(\eta_{ct})(K_1 \oplus K_2)(d_1 \oplus d_2) \end{aligned} \tag{26}$$

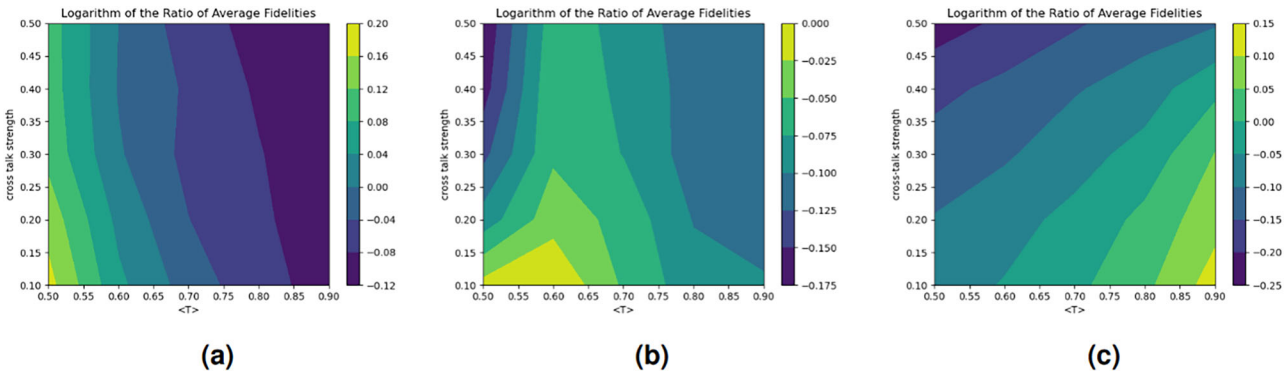

Fig. 6 | The behavior of the average fidelity in the presence of crosstalk for different amplification schemes. The color plots illustrate the average fidelity as a function of the average transmissivity $< T >$ in the x-axis and the crosstalk strength in the y-axis. The thermal noise is kept fixed to $n_{th} = 0.2$. **a** Average Fidelity ratio in the postprocessing amplification scenario. **b** Average Fidelity ratio in the post-amplification scenario. **c** Average Fidelity ratio in the pre-amplification scenario.

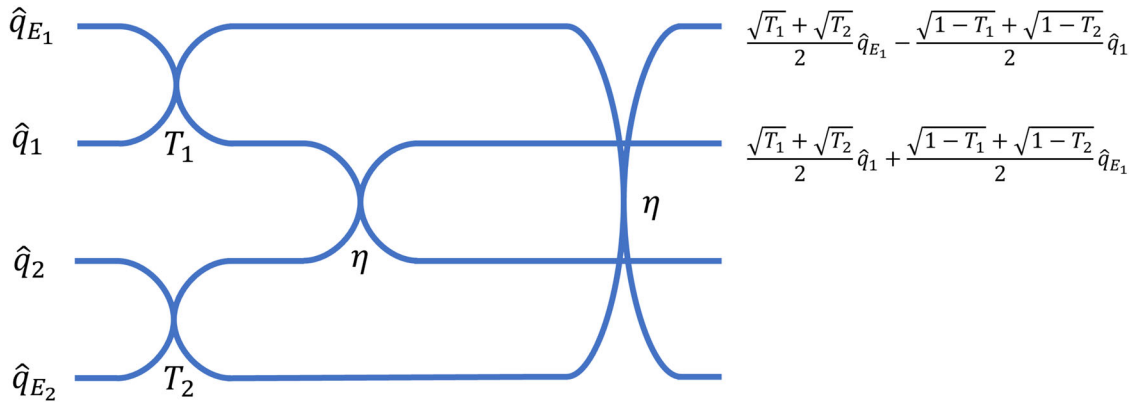

Fig. 7 | A diagram showing the evolution of the quadratures of different modes. The symbols $\hat{q}_1$ and $\hat{q}_2$ stand for the quadratures of the signal modes transmitted through the Gaussian channels. The Gaussian channels are represented by beam splitter interactions with transmissivities T_1 and T_2, respectively, with $\hat{q}_{E_1}$ and $\hat{q}_{E_2}$ standing for the attacker modes quadratures. The signal modes and the attacker modes are finally combined with 50: 50 beam splitters of transmissivity $\eta = \frac{1}{2}$. One of the signal modes is discarded as well as one of the attacker modes.

$$\begin{aligned} V_1 \oplus V_2 \to & B(\eta)B(\eta_{ct})\big[(A(G_1)\oplus A(G_2))\big[(K_1\oplus K_2)(V_1\oplus V_2)(K_1\oplus K_2)^T \\ & +(N_1\oplus N_2)\big](A(G_1)\oplus A(G_2))^T + N_{A(G_1)}\oplus N_{A(G_2)}\big]B(\eta_{ct})^T B(\eta)^T \\ d_1 \oplus d_2 \to & B(\eta)B(\eta_{ct})(K_1\oplus K_2)(A(G_1)\oplus A(G_2))(d_1\oplus d_2) \end{aligned} \tag{27}$$

$$\begin{aligned} V_1 \oplus V_2 \to & B(\eta)B(\eta_{ct})\big[(K_1\oplus K_2)\big[(A(G_1)\oplus A(G_2))(V_1\oplus V_2)(A(G_1)\oplus A(G_2))^T \\ & +N_{A(G_1)}\oplus N_{A(G_2)}\big](K_1\oplus K_2)^T + (N_1\oplus N_2)\big]B(\eta_{ct})^T B(\eta)^T \\ d_1 \oplus d_2 \to & B(\eta)B(\eta_{ct})(A(G_1)\oplus A(G_2))(K_1\oplus K_2)(d_1\oplus d_2) \end{aligned} \tag{28}$$

At the receiver side, after the two spatially-diverse signals are recombined using a beam splitter characterized by transmittivity η, only one of the output ports is used for measurement (homodyne or heterodyne) and further processing. The second output is discarded and treated as an effective loss, consistent with the prepare-and-measure framework commonly used in CV-QKD and CV communication systems. This approach simplifies both the analysis and implementation, while still allowing the receiver to benefit from the interference and averaging effects introduced by the recombination process. The measured output corresponds to the superposition of the two received modes and captures the diversity gain provided by the spatial-mode configuration. For the security analysis, we consider an entangling attack as highlighted in Fig. 7. Indeed, the scheme is equivalent to an entanglement-based scheme where Alice and Bob share a two-mode squeezed entangled state, hence the same security[20]. The mutual information $I(A{:}\,B)$ in this case is given by (see Appendix. A for derivation):

$$I(A:B) = \frac{v}{2}\log_2\left[1 + \frac{v\left(\frac{T1+T2}{2}\right)(V_{in}-1)}{1+\frac{1}{v}\left(1-\frac{T1+T2}{2}\right)(2n_{th}-1)}\right] \tag{29}$$

with $v = 1$ for homodyne detection and $v = 2$ for heterodyne detection. Moreover, to obtain the Holevo information, the reduced covariance matrices on the environment V_E and the covariance matrix of the environment conditioned on the measurement outcomes of Bob $V_{E|B}$ and their respective symplectic eigenvalues are needed. The environment covariance matrix V_E is given by (see Appendix B for derivation):

$$V_E = \begin{pmatrix} a\mathrm{I}_2 & c\sigma_z \\ c\sigma_z & b\mathrm{I}_2 \end{pmatrix} \tag{30}$$

with:

$$\begin{aligned} a &= \left(1-\frac{T1+T2}{2}\right)V_{in} + \frac{(T1+T2)}{2}\left(n_{th}+\frac{1}{2}\right) \\ b &= n_{th}+\frac{1}{2} \\ c &= \frac{(\sqrt{T1}+\sqrt{T2})}{\sqrt{2}}\left(\left(n_{th}+\frac{1}{2}\right)^2\right) - 1 \end{aligned} \tag{31}$$

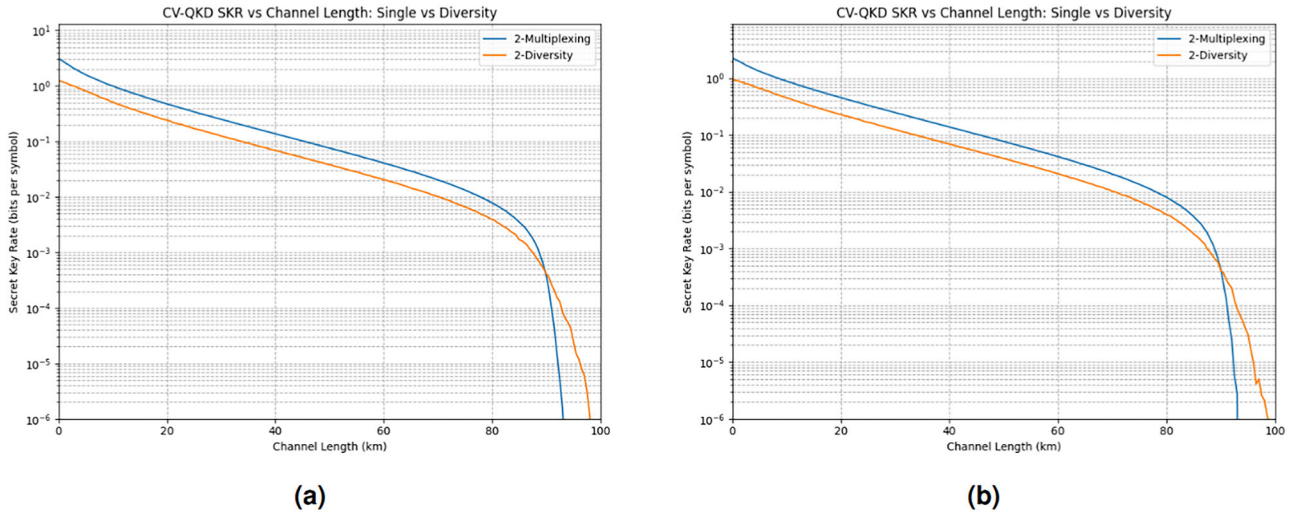

Fig. 8 | CV QKD secret key rate. a A benchmark between the secret key rate in the 2-diversity and the 2-multiplexing cases with heterodyne detection for perfect reconciliation efficiency and variance $V_{in} = 5/$. **b** A benchmark between the secret key rate in the 2-diversity and the 2-multiplexing cases with homodyne detection for perfect reconcilliation efficiency and variance $V_{in} = 5$.

The symplectic eigenvalues of this matrix are given by:

$$v_{\pm} = \frac{1}{2}(z \pm (b - a)) \tag{32}$$

where:

$$z = \sqrt{(a + b)^2 - 4c^2} \tag{33}$$

Differently, the conditional covariance matrix of the environment $V_{E|B}$ depends on the type of measurement. Due to the entropic equality:

$$S(E) - S(E|B) = S(AB) - S(A|B) \tag{34}$$

We focus on $V_{A|B}$ instead of $V_{E|B}$ We distinguish two cases, heterodyne detection and homodyne detection. For heterodyne detection, $V_{A|B}$ is given by[20]:

$$V_{E|B} = \left(k - \frac{g^2}{h+1}\right)\mathrm{I}_2 \tag{35}$$

with:

$$\begin{aligned} k &= V_{in} \\ h &= \left(\frac{T1+T2}{2}\right)(V_{in} - 1) + \left(n_{th} - \frac{1}{2}\right)\left(1 - \frac{T1+T2}{2}\right) + 1 \\ g &= \sqrt{\left(\frac{T1+T2}{2}\right)(V_{in}^2 - 1)} \end{aligned} \tag{36}$$

with symplectic eigenvalues:

$$v_{ht} = k - \frac{g^2}{h+1} \tag{37}$$

For homodyne detection, $V_{A|B}$ is given by[20]:

$$V_{A|B} = \begin{pmatrix} k - \frac{g^2}{h} & 0 \\ 0 & k \end{pmatrix} \tag{38}$$

with symplectic eigenvalue:

$$v_{hm} = \sqrt{k\left(k - \frac{g^2}{h}\right)} \tag{39}$$

The simulations of the average secret key rate in the presence of fading channels are reported in Fig. 8. To see the advantage of diversity in CV-QKD, we consider the 2-multiplexing case, where the QKD channel is bi-multiplexed without considering any interference effects or cross-talk between the two channels. Figure 8 compares the average secret key rates achieved under 2-diversity and 2-multiplexing configurations for both homodyne and heterodyne detection. In low- to moderate-loss regimes, the multiplexing scheme offers a higher key rate than the diversity scheme. This behavior is expected and can be attributed to the additivity of private (or secret key) capacity under separable signal encoding and separable measurement strategies, as assumed in our simulations. In such cases, each transmission path in the multiplexed setup contributes independently to the overall capacity, resulting in linear scaling of the secret key rate with the number of parallel channels.

In contrast, the diversity scheme distributes the signal across multiple spatial paths but ultimately recombines them into a single output, which is used for decoding. As a result, diversity does not benefit from the same scaling behavior. Instead, its strength lies in enhancing robustness: by statistically averaging over independently faded channels, diversity mitigates channel fluctuations and noise, leading to a more stable and reliable key rate, particularly in high-loss or turbulent environments. This highlights a fundamental trade-off: multiplexing favors throughput, while diversity prioritizes resilience, especially in scenarios where single-path transmission would fail to meet security thresholds.

Figure 9 further illustrates the performance of the diversity scheme as the number of spatially independent channels increases. A clear monotonic improvement in secret key rate is observed under both homodyne and heterodyne detection. This behavior aligns with theoretical expectations, as a greater number of i.i.d. fading paths reduces the likelihood of simultaneous deep fading, thereby improving the overall channel quality. Such diversity gain is particularly valuable in free-space optical links and other dynamic environments where bursty loss or atmospheric turbulence is prevalent. These results underscore the scalability and practical relevance of spatial-mode diversity for robust quantum communication under real-world impairments.

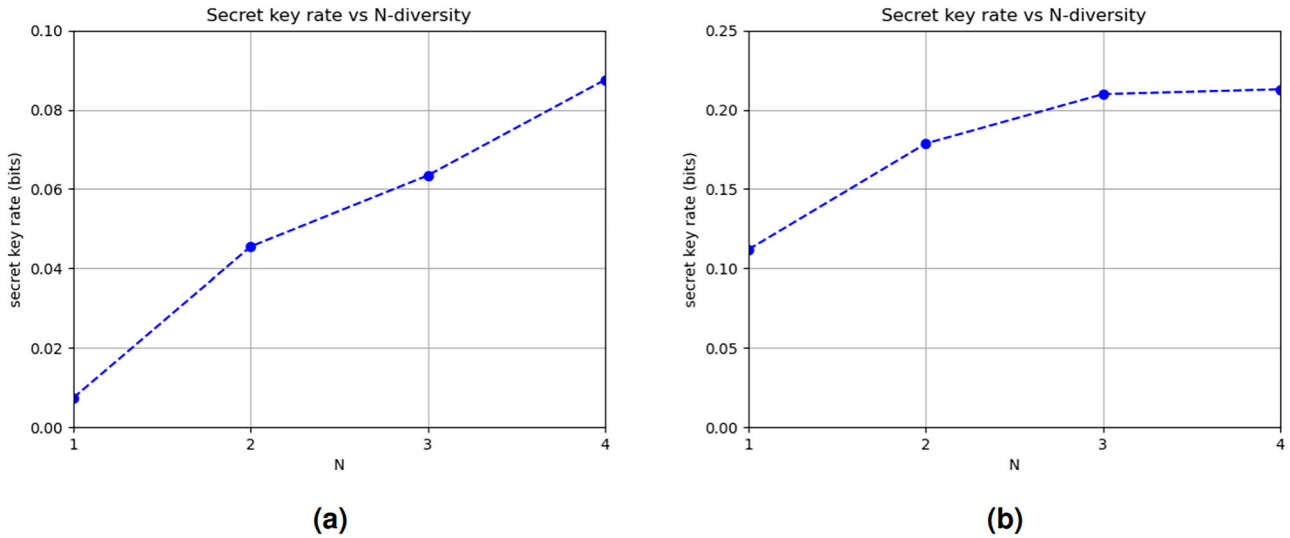

Fig. 9 | CV QKD secret key rate as function of N, the number of used channels for diversity. a The average secret key rate with heterodyne detection as a function of the number of used channels for diversity for variance V_{in} = 10 and 4db loss. **b** The average secret key rate with homodyne detection as a function of the number of used channels for diversity for variance V_{in} = 5 and 2db loss.

While diversity improves resilience to stochastic channel impairments such as fading, turbulence, and misalignment, it also introduces new considerations in terms of security. In particular, using additional spatial modes or degrees of freedom enlarges the system's Hilbert space, which may expose new vulnerabilities if not properly isolated. For example, imperfect mode separation or crosstalk could potentially be exploited by an adversary to extract information or compromise the integrity of the transmission. Therefore, any implementation of spatial-mode diversity must carefully account for the physical mode isolation and incorporate these effects into the security analysis. This balance between improved robustness and expanded attack surface is especially important in high-dimensional CV-QKD systems, where operational gains must not compromise composable security guarantees.

We should highlight that in addition to spatial-mode diversity, several alternative techniques have been proposed to mitigate noise in CV-QKD, such as *postselection*[21] and *trusted-noise modeling*[22]. Postselection-based methods enhance performance by discarding low-quality measurement outcomes, particularly those associated with deep fading or strong excess noise. While effective in boosting the secret key rate under certain conditions, postselection reduces the available data and often imposes stricter requirements on statistical estimation and reconciliation efficiency. Trusted-noise approaches, in contrast, assume that specific noise contributions (e.g., from detectors or internal components) are under the control of the legitimate parties and can be modeled securely. These require careful calibration and can complicate composable security proofs.

Spatial-mode diversity provides a complementary strategy that operates at the physical layer[4]. Rather than discarding data or adjusting trust assumptions, it reduces the impact of channel fluctuations by transmitting quantum signals across multiple statistically independent spatial paths. This reduces the probability that all modes simultaneously experience high loss or fading, thereby improving channel stability and average performance without reducing the data rate. Unlike postselection, all data can be retained, and the scheme integrates naturally with standard CV-QKD postprocessing. Moreover, diversity-based schemes can be combined with postselection or trusted-noise models to further enhance performance in highly dynamic or lossy environments.

Discussion

The investigation into spatial-mode diversity for CV quantum communications under realistic noise and channel conditions has yielded important insights into the potential of diversity to enhance fidelity and robustness in quantum information transfer. By integrating amplification strategies tailored to available CSI, this study presents a novel insight into how diversity outperforms traditional single-path or multiplexed schemes in adverse environments.

The performance improvements observed under strong fading and thermal noise conditions substantiate the core hypothesis that spatial-mode diversity mitigates the effects of stochastic channel behavior. The improvement in fidelity under 2-diversity configurations, across post-processing, post-amplification, and pre-amplification regimes, supports prior theoretical assertions about diversity in quantum communications[17,18]. Among these, the postprocessing amplification scheme, which avoids introducing noise to the quantum signal, demonstrates the most pronounced fidelity advantage under strong fading. This aligns with the broader understanding in classical and quantum communication theory that passive, post-measurement mitigation techniques are often less invasive and hence more noise-tolerant than pre- or active amplification methods.

Nevertheless, practical deployment reveals limitations to this advantage. The presence of modal crosstalk introduces a significant constraint. While spatial diversity retains performance benefits under moderate crosstalk, the degradation in fidelity becomes apparent, particularly in post-amplification scenarios. This is because active amplification not only enhances the signal but also amplifies accompanying noise, an effect well documented in quantum communication systems[16]. These findings underscore the importance of maintaining strong mode isolation or implementing compensation strategies in real-world platforms, especially in free-space optical systems where spatial orthogonality is not guaranteed. These observations build upon earlier studies which emphasized caution in mode-division multiplexing under non-ideal conditions[14,15], extending the analysis to the CV regime where Gaussian noise models and phase-space representations introduce unique considerations.

A particularly valuable contribution of this study lies in its comparative analysis of diversity and multiplexing strategies in CV-QKD. While multiplexing enables throughput gains due to linear capacity scaling with independent channels, diversity enhances transmission reliability. This trade-off was quantified using secret key rate comparisons under fading, revealing that diversity surpasses multiplexing performance in high-loss regimes. Such behavior mirrors the well-known diversity-multiplexing trade-off observed in classical MIMO systems and supports recent proposals for Quantum MIMO architectures[18], where reliability and rate must be carefully balanced. In CV systems, multiplexing benefits from separable encoding and detection, yielding additive key rate improvements, while

diversity leverages statistical averaging and constructive interference for enhanced robustness. These results complement multicarrier CV-QKD frameworks[23,24], suggesting that diversity can act as a physical-layer reliability enhancer in otherwise multiplexed or multicarrier schemes. Our key rate analysis follows the standard slow-fading model, averaging mutual and Holevo information over the fading distribution. An alternative, more conservative scenario would require the legitimate parties to operate under the worst-case mutual information–e.g., at minimum transmissivity–while granting the eavesdropper knowledge of the exact transmittance per channel use. This approach could yield a tighter lower bound on secure key rates and represents a potential direction for future security analysis.

Scalability is another critical consideration. The monotonic key rate improvement with increasing numbers of diversity channels is particularly promising for free-space and satellite-based QKD systems, where fading and turbulence are dominant impairments. Spatial-mode diversity offers a mechanism to stabilize performance in such environments without sacrificing throughput or resorting to complex postselection. These findings align with current architectural proposals for the quantum internet[25,26], where communication must remain robust across heterogeneous and dynamic link configurations–including fiber, free-space, and relay-based segments. In such networks, diversity enhances robustness not only against noise but also potentially against adversarial disruptions, assuming secure mode isolation can be maintained. This positions spatial-mode diversity as a candidate enabling technology for future quantum internet infrastructures, where reliable operation of entanglement distribution, teleportation, and distributed quantum computation is essential.

Finally, this work opens doors for broader integration of diversity into CV quantum communications beyond standard Gaussian protocols. Hybrid discrete-variable-continuous-variable (DV-CV) systems[27,28], particularly those aimed at entanglement distribution and repeater networks, may benefit from the robustness offered by spatial-mode diversity. Future studies could investigate how diversity interfaces with non-Gaussian operations and quantum error correction. Altogether, this study lays both an empirical and theoretical foundation for incorporating diversity into the physical layer of quantum communication systems, highlighting its practical promise, potential limitations, and relevance to the design of scalable, secure, and resilient quantum networks.

Conclusion

In this work, we have investigated the potential of spatial-mode diversity to enhance the performance and resilience of continuous-variable quantum communication systems operating under realistic channel impairments such as fading, thermal noise, and crosstalk. By analyzing different amplification strategies–postprocessing, post-amplification, and pre-amplification–we demonstrate that diversity can significantly improve the fidelity of transmitted quantum states and stabilize performance in adverse conditions. Our analysis reveals that in high-loss or noisy environments, spatial-mode diversity outperforms traditional single-channel transmission and even multiplexing schemes in terms of average secret key rate. This advantage becomes especially relevant in continuous-variable quantum key distribution, where robustness to environmental fluctuations is critical for maintaining security. These results suggest that spatial-mode diversity, as a physical-layer technique, offers a promising path toward scalable and reliable quantum networks. Future work may explore its integration with trusted-noise models, postselection strategies, and its extension to hybrid or non-Gaussian protocols within the broader context of the quantum internet.

Methods

Here we give an overview of the main techniques used to establish our results.

Channel Model

We consider Gaussian Lossy channels $\mathscr{G}[T, n_{th}]$, described by a transmissivity T and thermal noise characterized by the thermal background average number of photons n_{th}. The channel acts on a Gaussian state ρ of covariance matrix V and mean vector d as[29]:

$$\begin{aligned} \rho &\to \mathscr{G}[T, n_{th}](\rho) \\ V &\to TV + (1-T)\left(n_{th} + \frac{1}{2}\right)\mathrm{I}_2 \\ d &\to \sqrt{T}d \end{aligned} \tag{40}$$

with I_2 being the two-dimensional identity matrix. Here, V denotes the covariance matrix and d is the mean vector of the Gaussian state ρ, defined as:

$$V_{ij} = \frac{1}{2}\langle\{\hat{R}_i, \hat{R}_j\}\rangle - \langle\hat{R}_i\rangle\langle\hat{R}_j\rangle, \tag{41}$$

$$d_i = \langle\hat{R}_i\rangle, \tag{42}$$

where $\hat{R} = (\hat{q}_1, \hat{p}_1, \hat{q}_2, \hat{p}_2, \ldots)^T$ is the vector of quadrature operators and $\{A, B\} = AB + BA$ denotes the anti-commutator. The average or expectation value of an operator $\hat{O}$ with respect to a quantum state ρ is defined as:

$$\langle\hat{O}\rangle = Tr(\rho\hat{O}). \tag{43}$$

Alternatively, for continuous-variable systems described by Wigner functions, the average of an operator $\hat{O}$ can be expressed as an integral over phase space:

$$\langle\hat{O}\rangle = \int W(\chi)\, O_W(\chi)\, d^{2n}\chi$$

In particular, the components of the mean vector d and the covariance matrix V are given by:

$$d_i = \int \chi_i W(\chi)\, d^{2n}\chi, \quad V_{ij} = \int \chi_i\chi_j W(\chi)\, d^{2n}\chi - d_i d_j$$

where $W(\chi)$ is the Wigner function of the state, and χ denotes a point in phase space. For a quantum state ρ, the Wigner function $W(\chi)$ is a quasi-probability distribution in phase space. In the case of a Gaussian state with mean vector $\mathbf{d} \in \mathbb{R}^{2n}$ and covariance matrix $V \in \mathbb{R}^{2n\times 2n}$, the Wigner function is given by:

$$W(\chi) = \frac{1}{\pi^n\sqrt{\det V}}\exp\left[-(\chi-\mathbf{d})^\top V^{-1}(\chi-\mathbf{d})\right], \tag{44}$$

where $\chi \in \mathbb{R}^{2n}$ is the real-valued phase space coordinate vector, n is the number of modes, and $\det V$ is the determinant of the covariance matrix. This expression fully characterizes the Gaussian state and is used to compute the fidelity between input and output states by evaluating the overlap of their corresponding Wigner functions. The fading of the channel transmittance is modeled by a log-normal distribution, characterized by the probability density function:

$$f_T(T) = \frac{1}{T\sigma\sqrt{2\pi}}\exp\left(-\frac{(\ln T - \mu)^2}{2\sigma^2}\right),$$

where $T \in (0, 1)$ denotes the channel transmittance, μ is the mean of $\ln T$, and σ is its standard deviation. The parameters μ and σ are chosen such that the average transmittance $\langle T\rangle$ corresponds to the desired loss level.

In our diversity-based model, each quantum signal traverses an independent Gaussian lossy channel with transmittance T_1 and T_2, respectively. The action of each channel on the covariance matrix and displacement vector can be described using affine transformations in phase space.

Specifically, the matrices K_1 and K_2 represent the linear part of the channel transformation and are defined as:

$$K_i = \sqrt{T_i} \cdot \mathbb{I}_2,$$

where $\mathbb{I}_2$ is the 2×2 identity matrix, and $i \in \{1, 2\}$. This corresponds to the standard Gaussian lossy channel, where each quadrature is attenuated by a factor of $\sqrt{T_i}$.

The associated noise matrices N_1 and N_2, accounting for thermal noise in the environment, are given by:

$$N_i = (1 - T_i)\left(2n_{\text{th}} + 1\right) \cdot \mathbb{I}_2,$$

where n_{th} is the mean thermal photon number. Together, (K_i, N_i) define the action of each channel on Gaussian states as part of the full diversity system.

Gaussian amplification

The process of a physical active amplification $\mathscr{A}[G]$ of the signal with amplification gain G is described by a Gaussian channel that transforms the original state by[29]:

$$\rho \to \mathscr{A}[G](\rho) \tag{45}$$

$$V \to GV + (G - 1)\mathrm{I}_2 \tag{46}$$

$$d \to \sqrt{G}d \tag{47}$$

The term $(G - 1)\mathrm{I}_2$ reflects that the active physical amplification is a noisy process.

Crosstalk

Crosstalk in communications can arise in various scenarios and is typically due to interference between signal paths. As the optical signal propagates through free space, the light beam can diverge due to diffraction. If the beams from different transmitters are not sufficiently collimated or if they diverge too much, they can overlap at the receiver, causing crosstalk. Moreover, variations in the refractive index of the atmosphere caused by temperature fluctuations and air movement can lead to beam wandering and spreading. Similarly, crosstalk in multicore fibers (MCFs) primarily arises from core-to-core coupling due to the close proximity of the cores, where overlapping evanescent fields cause optical modes in one core to couple into adjacent cores. This issue is exacerbated by refractive index fluctuations, geometry non-uniformities, and mechanical stresses such as fiber bending and external forces. Additionally, propagation effects like differential mode delay and random perturbations can dynamically influence crosstalk levels. Crosstalk can also vary with wavelength and modal characteristics. Crosstalk can cause parts of the beam to stray into the path of another receiver. The crosstalk in this paper is modeled as a beam splitter $B(\eta)$ with η being its transmissivity. The $B(\eta)$ representation on phase space is given by the symplectic matrix:

$$B(\eta) = \begin{pmatrix} \sqrt{\eta}\mathrm{I}_2 & -\sqrt{1-\eta}\mathrm{I}_2 \\ \sqrt{1-\eta}\mathrm{I}_2 & \sqrt{\eta}\mathrm{I}_2 \end{pmatrix} \tag{48}$$

The action of the beam splitter on the covariance matrix V and the mean vector d of a given state is described as:

$$V \to B(\eta)VB(\eta)^T \tag{49}$$

$$d \to B(\eta)d \tag{50}$$

Figures of Merit

Here we present the figures of merit used in **Results** to benchmark our diversity scheme.

Fidelity. We benchmark the advantage of the scheme in terms of the average fidelity in the 2-diversity and the 0-diversity scenarios, where the latter denotes single transmission. The fidelity between the output state and input state with Wigner functions $W_{out}(\chi)$ and $W_{in}(\chi)$ as:

$$F(\rho_{out}, \rho_{in}) = (2\pi)^n \int W_{out}(\chi) W_{in}(\chi) d\chi \tag{51}$$

where n is the number of modes of the states. For two Gaussian states, ρ_{in} and ρ_{out} of phase space representation $(V1, d1)$ and $(V2, d2)$ respectively, the fidelity expression simplifies to:

$$F(\rho_{out}, \rho_{in}) = \frac{\exp\left(-\frac{(d1-d2)(V1+V2)(d1-d2))^T}{2}\right)}{\sqrt{\det(V1 + V2)}} \tag{52}$$

In a realistic communications scenario, the mean vectors and the covariance matrices of the output states ρ_{out} depend on the stochastic transmissivity parameter. As a matter of fact, we define the average fidelity between the output and input states by:

$$F_{avg} = \int f_T(T) F(\rho_{out}(T), \rho_{in}(T)) dT \tag{53}$$

We should highlight that we use fidelity as a physical-layer performance metric to evaluate the robustness of quantum states under fading and noise. Although not directly used in CV-QKD security proofs, it provides insight into state degradation before post-processing and is very useful when we extend the work to quantum entanglement distribution using CV encodings[28]. The secret key rate remains our primary security-relevant benchmark.

Secret key rate. The secret key rate is a crucial figure of merit in the evaluation of diversity schemes in QKD. It quantifies the number of secure bits that can be extracted per channel use and directly reflects both the efficiency and the security of the quantum key distribution system. In practical deployments–particularly in dynamically varying environments such as free-space optical links or atmospheric channels–secret key rate estimates must take into account statistical fluctuations in channel transmittance, noise, and eavesdropping vulnerability.

Diversity schemes, which leverage multiple independent transmission paths or degrees of freedom, aim to mitigate these impairments and improve the stability of the communication channel. When the channel exhibits random fading–such as lognormally distributed transmittance due to atmospheric turbulence–the average secret key rate serves as a natural performance metric for characterizing system robustness. It allows for comparison between different diversity strategies and provides insight into how effectively the system can sustain secure communication under realistic, non-stationary conditions.

In this work, we assume a *slow fading regime*, as formalized in ref. 30, in which the channel transmittance remains constant over a block of transmissions, and its distribution $f_T(T)$ is either known or empirically estimated. This assumption allows us to define the average asymptotic secret key rate as:

$$K = \int f_T(T) \left[\beta I(A:B)(T) - \chi(E:B)(T)\right] dT, \tag{54}$$

where β is the reconciliation efficiency, $I(A{:}\,B)$ is the mutual information between Alice and Bob for a given transmittance T, and $\chi(E{:}\,B)$ is the Holevo

information between Eve and Bob, characterizing the maximum information that an eavesdropper can extract.

The Holevo information is given by:

$$\chi(E:B) = S(E) - S(E|B), \tag{55}$$

where $S(E)$ is the von Neumann entropy of Eve's reduced state (holding the purification of the system), and $S(E|B)$ is the conditional entropy after Bob's measurement.

For Gaussian states, the entropy is computed from the symplectic eigenvalues ν_i of the corresponding covariance matrix V, and the total entropy is expressed as:

$$S(V) = \sum_i g(\nu_i), \tag{56}$$

where the entropy function $g(x)$ is defined by:

$$g(x) = \frac{x+1}{2}\log_2\left(\frac{x+1}{2}\right) - \frac{x-1}{2}\log_2\left(\frac{x-1}{2}\right). \tag{57}$$

This framework enables us to evaluate the expected long-term key rate performance of CV-QKD systems under statistical fading and supports the assessment of physical-layer techniques such as spatial-mode diversity.

The mutual information $I(A:B)$

Assuming the modulation variance at the sender Alice being V_{in}, then after transmission of the state through a bosonic Gaussian channel the covariance matrix undergoes the following transformation:

$$V_{in} \to TV_{in} + \left(n_{th} + \frac{1}{2}\right)\mathrm{I}_2 \tag{58}$$

as specified in Eq. (40). In a diversity scheme setup, and in the presence of two parallel channels with similar combining of Fig. 1 after discarding the local oscillator state, the covariance matrix evolves as:

$$V_{in} \to \frac{T_1+T_2}{2}V_{in} + \left(1 - \frac{T_1+T_2}{2}\right)\left(n_{th} + \frac{1}{2}\right)\mathrm{I}_2 \tag{59}$$

for homodyne detection, and

$$V_{in} \to \frac{1}{2}\left[\frac{T_1+T_2}{2}V_{in} + \left(1 - \frac{T_1+T_2}{2}\right)\left(n_{th} + \frac{1}{2}\right)\mathrm{I}_2\right] + \frac{1}{4}\mathrm{I}_2 \tag{60}$$

for heterodyne detection. The mutual information is defined as

$$I(A:B) = \frac{\nu}{2}\log_2(1+SNR) \tag{61}$$

with SNR being the signal-to-noise ratio and ν is a factor identical to 2 for heterodyne detection and 1 for homodyne detection. From Eqs. (59) and (60), we can deduce the SNR for both homodyne and heterodyne detections and it is given respectively by:

$$SNR = \frac{\nu\left(\frac{T1+T2}{2}\right)\left(V_{in}-1\right)}{1+\frac{1}{\nu}\left(1-\frac{T1+T2}{2}\right)(2n_{th}-1)} \tag{62}$$

therefore the mutual information is given by:

$$I(A:B) = \frac{\nu}{2}\log_2\left[1 + \frac{\nu\left(\frac{T1+T2}{2}\right)(V_{in}-1)}{1+\frac{1}{\nu}\left(1-\frac{T1+T2}{2}\right)(2n_{th}-1)}\right] \tag{63}$$

The covariance matrix of the environment

To understand the derivation of the covariance matrix of the environment V_E in Eq. (30), we follow the diagram in Fig. 7 reflecting the evolution of the quadratures in the presence of an environment which is controlled by the attacker. The quadratures $\hat{q}_1$ and $\hat{q}_2$ stand for the signal modes that are transmitted through two parallel Gaussian channels for the 2-diversity scheme. The two Gaussian channels are explicitly represented by beam splitter interactions of the signal modes with the corresponding attacker modes, $\hat{q}_{E_1}$ and $\hat{q}_{E_2}$ with transmissivities T_1 and T_2, respectively. The signal modes are combined at the receiver by a 50: 50 beam splitter, and the same for the attacker modes. At the end of the process, one of the signal modes is discarded as well as one of the attacker modes, reflecting a cloning attack. The quadratures of the remaining signal and environment mode are given by:

$$\hat{q}_B = \frac{\sqrt{T_1}+\sqrt{T_2}}{2}\hat{q}_1 + \frac{\sqrt{1-T_1}+\sqrt{1-T_2}}{2}\hat{q}_{E_1} \tag{64}$$

$$\hat{q}_{E_o} = \frac{\sqrt{T_1}+\sqrt{T_2}}{2}\hat{q}_{E_1} - \frac{\sqrt{1-T_1}+\sqrt{1-T_2}}{2}\hat{q}_1 \tag{65}$$

By setting $\langle\hat{q}_{E_1}^2\rangle = \langle\hat{p}_{E_1}^2\rangle = (n_{th}+\frac{1}{2})$ and $\langle\hat{q}_1^2\rangle = \langle\hat{p}_1^2\rangle = V_{in}$, the covariances and the cross covariances of an entangled attacker are given by:

$$\begin{aligned}
\langle\hat{q}_{E_o}^2\rangle &= \langle\hat{p}_{E_o}^2\rangle = \frac{T_1+T_2}{2}\left(n_{th}+\frac{1}{2}\right) + \left(1-\frac{T_1+T_2}{2}\right)V_{in}\\
\langle\hat{q}_{E_o}\hat{q}_E\rangle &= -\langle\hat{p}_{E_o}\hat{p}_E\rangle = \frac{\sqrt{T_1}+\sqrt{T_2}}{2}\langle\hat{q}_{E_1}\hat{q}_E\rangle\\
&= \frac{\sqrt{T_1}+\sqrt{T_2}}{2}\sqrt{\left(n_{th}+\frac{1}{2}\right)^2 - 1}\\
\langle\hat{q}_E^2\rangle &= \langle\hat{p}_E^2\rangle = \left(n_{th}+\frac{1}{2}\right)
\end{aligned} \tag{66}$$

with $\hat{q}_E$ and $\hat{p}_E$ being the quadratures of the entangling attacker mode. As a result, the covariance matrix of the environment is:

$$V_E = \begin{pmatrix} a\mathrm{I}_2 & c\sigma_z \\ c\sigma_z & b\mathrm{I}_2 \end{pmatrix} \tag{67}$$

with:

$$\begin{aligned}
a &= \left(1-\frac{T1+T2}{2}\right)V_{in} + \frac{(T1+T2)}{2}\left(n_{th}+\frac{1}{2}\right)\\
b &= n_{th}+\frac{1}{2}\\
c &= \sqrt{\frac{(T1+T2)}{2}\left(\left(n_{th}+\frac{1}{2}\right)^2 - 1\right)}
\end{aligned} \tag{68}$$

Data availability

Data sharing not applicable to this article as no datasets were generated or analyzed during the current study.

Received: 28 October 2024; Accepted: 4 August 2025;
Published online: 25 August 2025

References

1. Braunstein, S. L. & Van Loock, P. Quantum information with continuous variables. *Rev. Mod. Phys.* **77**, 513–577 (2005).

2. Zhang, Y., Bian, Y., Li, Z., Yu, S. & Guo, H. Continuous-variable quantum key distribution system: Past, present, and future. *Appl. Phys. Rev.* **11**, 011318 (2024).
3. Andersen, U. L., Leuchs, G. & Silberhorn, C. Continuous-variable quantum information processing. *Laser Photonics Rev.* **4**, 337–354 (2010).
4. Koudia, S. et al. Physical layer aspects of quantum communications: A survey. arXiv e-prints arXiv–2407 (2024).
5. Leverrier, A., García-Patrón, R., Renner, R. & Cerf, N. J. Security of continuous-variable quantum key distribution against general attacks. *Phys. Rev. Lett.* **110**, 030502 (2013).
6. Jouguet, P., Kunz-Jacques, S. & Leverrier, A. Long distance continuous-variable quantum key distribution with a Gaussian modulation. arXiv **2011** (2011).
7. Jouguet, P., Kunz-Jacques, S., Leverrier, A., Grangier, P. & Diamanti, E. Experimental demonstration of long-distance continuous-variable quantum key distribution. *Nat. Photonics* **7**, 378–381 (2013).
8. Vasylyev, D., Semenov, A. & Vogel, W. Atmospheric quantum channels with weak and strong turbulence. *Phys. Rev. Lett.* **117**, 090501 (2016).
9. Vasylyev, D., Vogel, W. & Moll, F. Satellite-mediated quantum atmospheric links. *Phys. Rev. A* **99**, 053830 (2019).
10. Pirandola, S. & Papanastasiou, P. Improved composable key rates for CV-QKD. *Phys. Rev. Res.* **6**, 023321 (2024).
11. Koudia, S. The quantum internet: an efficient stabilizer states distribution scheme. *Phys. Scr.* **99**, 015115 (2023).
12. Dias, J., Winnel, M. S., Hosseinidehaj, N. & Ralph, T. C. Quantum repeater for continuous-variable entanglement distribution. *Phys. Rev. A* **102**, 052425 (2020).
13. Choi, I., Young, R. J. & Townsend, P. D. Quantum key distribution on a 10gb/s wdm-pon. *Opt. Express* **18**, 9600–9612 (2010).
14. Zhou, Y. et al. Multiprobe time reversal for high-fidelity vortex-mode-division multiplexing over a turbulent free-space link. *Phys. Rev. Appl.* **15**, 034011 (2021).
15. Xavier, G. B. & Lima, G. Quantum information processing with space-division multiplexing optical fibres. *Commun. Phys.* **3**, 9 (2020).
16. Eriksson, T. A. et al. Crosstalk impact on continuous variable quantum key distribution in multicore fiber transmission. *IEEE Photonics Technol. Lett.* **31**, 467–470 (2019).
17. Yuan, R. & Cheng, J. Free-space optical quantum communications in turbulent channels with receiver diversity. *IEEE Trans. Commun.* **68**, 5706–5717 (2020).
18. ur Rehman, J., Oleynik, L., Koudia, S., Bayraktar, M. & Chatzinotas, S. Diversity and multiplexing in quantum MIMO channels. *EPJ Quantum Technol*. **12**, 18 (2025).
19. Anipeddi, N. L., Horgan, J., Oi, D. K. & Kilbane, D. Optical ground station diversity for satellite quantum key distribution in Ireland. *EPJ Quantum Technol*. **12**, 91 (2025).
20. Laudenbach, F. et al. Continuous-variable quantum key distribution with Gaussian modulation theory of practical implementations. *Adv. Quantum Technol.* **1**, 1800011 (2018).
21. Kish, S. P. et al. Mitigation of channel tampering attacks in continuous-variable quantum key distribution. *Phys. Rev. Res.* **6**, 023301 (2024).
22. Shao, Y. et al. Phase noise model for continuous-variable quantum key distribution using a local local oscillator. *Phys. Rev. A* **104**, 032608 (2021).
23. Gyongyosi, L. Multicarrier continuous-variable quantum key distribution. *Theor. Comput. Sci.* **816**, 67–95 (2020).
24. Gyongyosi, L. & Imre, S. Multiple access multicarrier continuous-variable quantum key distribution. *Chaos Solitons Fractals* **114**, 491–505 (2018).
25. Koudia, S., Cacciapuoti, A. S. & Caleffi, M. Deterministic generation of multipartite entanglement via causal activation in the quantum internet. *IEEE Access* **11**, 73863–73878 (2023).
26. Gyongyosi, L. & Imre, S. Advances in the quantum internet. *Commun. ACM* **65**, 52–63 (2022).
27. Koudia, S. & Gharbi, A. Quantum non-gaussianity from an indefinite causal order of Gaussian operations. *Int. J. Quantum Inf.* **19**, 2150026 (2021).
28. Koudia, S. & Chatzinotas, S. Crosstalk-resilient quantum MIMO for scalable quantum communications. arXiv preprint arXiv:2506.21704 (2025).
29. Ferraro, A., Olivares, S. & Paris, M. G. Gaussian states in continuous variable quantum information. arXiv preprint quant-ph/0503237 (2005).
30. Papanastasiou, P., Weedbrook, C. & Pirandola, S. Continuous-variable quantum key distribution in uniform fast-fading channels. *Phys. Rev. A* **97**, 032311 (2018).

Acknowledgements

This work was supported by the project Lux4QCI (GA 101091508) funded by the Digital Europe Program, and the project LUQCIA, funded by the European Union - Next Generation EU, with the collaboration of the Department of Media, Connectivity and Digital Policy of the Luxembourgish Government in the framework of the RRF program. The authors thank Dr. Mert Bayraktar for discussions.

Author contributions

S.K. carried out the analysis and wrote the paper. S.K., L.O., J.U., and S.C. discussed the methods and the results and revised the manuscript. S.C. supervised the work.

Competing interests

The authors declare no competing interests.

Additional information

Correspondence and requests for materials should be addressed to Seid Koudia.

Peer review information *Communications Physics* thanks the anonymous reviewers for their contribution to the peer review of this work.

Reprints and permissions information is available at http://www.nature.com/reprints

Publisher's note Springer Nature remains neutral with regard to jurisdictional claims in published maps and institutional affiliations.